RPCA with Log-Schatten Norm and Adaptive Histogram Equalization for Medical Imaging

Habte Tadesse Likassa and Ding Geng Chen*

College of Health Solutions, Arizona State University, USA

Abstract: Medical imaging, especially cancer and retinal fundus analysis, is often compromised by artifacts and heavy noise and artifact, which can hinder accurate diagnosis. Existing low-rank sparse component methods, such as RPCA with the conventional nuclear norm, assume uniform singular value weights, which may not hold true due to noise variations in images. We recently developed RPCA with the log-weighted nuclear norm, which addresses some of these issues but still relies on weight selection, potentially introducing bias. To overcome these limitations, we propose a novel method that integrates RPCA with Log-Schatten Norm (LSN) and Adaptive Histogram Equalization (AHE) for medical imaging and clinical purposes. The Log-Schatten Norm improves singular value penalization and structure preservation, while AHE enhances contrast and reduces noise. The method is formulated as an optimization problem and solved using the Alternating Direction Method for Multipliers (ADMM). Experimental results on publicly available retinal and cancer image datasets demonstrate that our method outperforms existing methods in enhancing overall image quality, making it a promising tool for medical imaging applications.

Keywords: RPCA, Log-Schatten Norm, AHE, Medical Imaging and ADMM.

1. INTRODUCTION

Medical image processing is crucial for detecting various anomalies, helping medical experts use to conduct successful clinical experiments, improving cancer detection, and enhancing the quality of retinal fundus images [1]. Developing a new method to enhance the true underlying structure medical imaging is essential for early screening and treatment planning. One of the most challenging issues is analyzing high-dimensional medical image data that is impaired by artifacts and noise [2-4]. This phenomenon arises in various scenarios, such as medical image enhancement, surveillance, and healthcare [5]. Therefore, it is vital to develop a new method that can recover degraded medical images from corrupted ones, and is robust against adverse effects like artifacts, errors, and noise.

Several methods have been developed to enhance the quality of medical images [6-10], particularly for neuroimaging data analysis [11-13]. For example, [14-18] proposed hybrid methods for retinal image enhancement. However, these approaches did not specifically address the detailed features of retinal images. To tackle these challenges, [19] introduced a unified framework method, which combines retinal image enhancement with vessel segmentation. Another innovative technique by [20] uses a three channel eye fundus image as input and outputs the severity of diabetic retinopathy, though it fails to provide detailed characteristics of the images. Recently, Habte *et al*. [21] developed a RPCA method that improves the quality of retinal fundus images by incorporating the log-weighted nuclear norm instead of the classical nuclear norm, denoted by L. However, this method heavily depends on the weights in singular value decomposition. A key limitation of the RPCA method is that it is purely global-based for image enhancement. Despite its improvements, this method lacks detailed retinal image characterization, limiting its ability to fully capture the complexity of the data for clinical use. Moreover, clinical fundus images often face issues such as uneven illumination, blur, and artifacts caused by equipment or environmental factors [19]. Additionally, [22] proposed sparse and low-rank matrix decompositions for image recovery, and novel methods [23,24] have been introduced to enhance the quality of retinal fundus images. However, their performance remains suboptimal, as they fail to capture the detailed retinal features and do not effectively address noise and degradation in diabetic retinal images. Furthermore, [25] proposed a multimodal method that uses self-supervised learning for multimodal representation to enhance retinal imaging. To further improve retinal image quality, we recently developed a robust PCA method [26] that incorporates contrast-limited adaptive histogram equalization (CLAHE). This method demonstrated superior image enhancement compared to baseline approaches, offering a promising solution for enhancement. Additionally, [11] proposed a Robust PCA method based on adaptive weighted least squares and low-rank matrix factorization (AWLSLR) for image reconstruction. Recently, low-rank sparse decomposition has been proposed for medical image

*Address correspondence to this author at the College of Health Solutions, Arizona State University, USA; Email: Ding-Geng.Chen@asu.edu

processing [26,27], though their performance has yet to show significant improvement.

A variety of algorithms have been reported to address cancer-related issues in medical images [28-30]. For example, [31] proposed an advanced machine learning technique for prostate cancer imaging, while [32] introduced a novel method for time-dependent ROC curve analysis in medical research to detect cancer in related datasets. However, these approaches lack robustness when handling noisy multi-array data. Therefore, it is crucial to develop a novel method that addresses these challenges and enhances the quality of medical images, particularly cancer-related images, to improve clinical applications and diagnostic accuracy.

In this paper, we propose a novel method that significantly enhances the quality of medical images, particularly retinal and cancer images. Developing robust image enhancement techniques capable of recovering degraded images is crucial, especially when faced with challenges such as occlusions and variations in illumination. To make the method more resilient to artifacts and noise, we introduce a new method by integrating RPCA with LSN and AHE. RPCA with LSN greatly improves image quality by effectively denoising and capturing key features, while AHE enhances contrast, especially in degraded images, ensuring clearer and more accurate detection. In this work, we incorporate LSN into the RPCA framework to better recover the true underlying structure, overcoming the limitations of the classical nuclear norm (which assigns equal weights to singular values) and the log-weighted nuclear norm (which is heavily dependent on weight selection). Furthermore, existing RPCA methods fail to capture the detailed characteristics of medical images required for clinical applications. To address this limitation and make the new method more robust, we integrate AHE into the RPCA framework. To the best of our knowledge, this is the first method to combine a low-rank sparse component technique with LSN and AHE for medical image processing within the RPCA framework. Thus, this problem is formulated as an optimization problem, with parameters solved using ADMM in a round-robin manner. The key contributions of this paper based on the integration of LSN and AHE within the RPCA framework are outlined as follows:

- In this paper, we propose the Log-Schatten norm, which offers a significant advantage over existing nuclear and log-weighted nuclear norms by better preserving structural details and reducing noise in medical images. This norm enhances retinal and cancer detection images, maintains critical features for early disease detection, and improves accuracy in identifying malignancies, all while effectively handling distortions like poor contrast and artifacts.
- Then, the AHE is integrated within the RPCA framework to enhance fine details and improve the visibility of key anatomical features.
- By combining these two novel tools—Log-Schatten Norm and AHE within the RPCA framework, our method achieves superior image recovery compared to the state-of-the-art methods based on the cancer and retinal image databases.

To facilitate understanding, a comparison between the proposed method and the baseline methods is summarized in Table **1**.

The remainder of this article is organized as follows: Section 2 presents the proposed method, while Section 3 describes the nature of the data. Section 4 presents the simulation results, and finally, Section 5 provides the conclusions and discussions.

2. PROPOSED METHOD

Consider n medical images, $\{\boldsymbol{I}_i^0\} \in \Re^{w\times h\times c}$, $i = 1,\cdots, n$, where w and h denote the width and height of the

Table 1: Summary Table of the Methods

Methods	Objective	Constraints	Norm Definition
RPCA [26, 27]	$\min_{L,E}\ (\|\|L\|\|L_{logw,*} + \lambda\|\|\ \varepsilon\ \|\|_{2,1})$	$M = L_{CLAHE} + \varepsilon$	$\|\|L\|\|L_{w,*} = \Sigma_i \log(\sigma_i)(L)$
AWLS-LR [11]	$\min_{U,V,S}\ \|\|M - UV - \varepsilon\ \|\|_F^2 + \lambda\|\|W \circ \varepsilon\ \|\|_F^2$	M = L + E	$\|\|M\|\|F = \sqrt{\sum_{i=1}^{m}\sum_{j=1}^{n}\|m_{ij}\|^2}$
Proposed Method	$\min_{L,E}\ (\|\|L\|\|_{Log-S} + \lambda\|\|\ \varepsilon\ \|\|_1)$	$M = L_{AHE} + \varepsilon$	$\|\|L\|\|_{\|\|Log-S} = \Sigma_i \log\ (\sigma_i^p)(L)$

images, respectively, and c represents the number of channels (e.g., c = 3 for an RGB image). These images are distorted due to outliers, noises, and artifacts.

Each of these retinal images indicates and exhibits high correlation with each other. Often, these images are corrupted by issues such as image blurring due to noises and uneven illuminations. Then, we can stack these images into a matrix: $\boldsymbol{M} = [vec(\boldsymbol{I}_1^0) \mid vec(\boldsymbol{I}_2^0) \mid \cdots \mid vec(\boldsymbol{I}_n^0)] \in \Re^{m \times n}$, where $vec(\cdot)$ denotes the vector stacking operator. We can decompose M into a summation of a low-rank component and a sparse error matrix [33]: $M = L + E$ [34], where $L \in \Re^{m \times n}$ is denoting the enhanced images, and $E^{m \times n}$ is the matrix incurred by noises and uneven illumination. Classical low-rank sparse component methods, such as RPCA [34] with an existing nuclear norm, assume uniform singular value weights, which may not hold due to the variation of the image noise and quality. Additionally, existing RPCA methods focus on global enhancement, but miss fine details in the retina.

To begin with, the RPCA [34] is formulated as follows:

$$\min_{\mathrm{L,E,Z}} \gamma \|\mathrm{L}\|_* + \lambda \|\mathrm{E}\|_1 \text{ s.t. } \mathrm{M} = \mathrm{L} + \mathrm{E} \tag{1}$$

Where $\|\mathrm{L}\|_*$ is the nuclear norm of L, which is the sum of the singular values of the low rank component. $\|E\|_1$ is the L_1 norm of E. λ is the regularization parameter that control the relative weight of the low-rank and sparse components. To address these drawbacks, we propose a novel method incorporating the CLAHE [26]. Since the log-weighted nuclear norm depends on weight selection, which may introduce bias and require careful tuning, we consider the log-Schatten norm as a better alternative, offering more balanced singular value penalization, improved low-rank approximation, and greater robustness to noise. Ultimately, the RPCA with the Log-Schatten norm for the low-rank component is given by:

$$\min_{\mathrm{L,E,Z}} \gamma \|\mathrm{L}\|_{Log-S} + \lambda \|\mathrm{E}\|_1 \text{ s.t. } \mathrm{M} = \mathrm{L} + \mathrm{E} \tag{2}$$

Where $\|L\|_{Log-S}$ is the Log-Schatten norm of L, which regularizes the low-rank component using a logarithmic shrinkage technique, λ and γ are updated regularization parameters, optimized to balance the low-rank and sparse components after the initial RPCA framework. Once the low-rank component L has been obtained from the optimization above, we apply AHE to enhance the low-rank component: $L_{AHE} = AHE(L)$ where L_{AHE} is the enhanced low-rank component after AHE has been applied, AHE enhances contrast, making fine details in the retinal image clearer and improving the overall visibility of structures in the image. For a given matrix L, let σ_i be its singular values (from Singular Value Decomposition, SVD: $L = U\Sigma V^T$, the Log-Schatten norm is defined as:

$$\|\mathrm{L}\|_{Log-\mathrm{S}} = \sum_i log(\sigma_i^p)(\mathrm{L}) \tag{3}$$

where σ_i are the singular values of L, r is the rank of L, the function $\|\mathrm{L}\|_{Log-S} = \sum_i log(\sigma_i^p)(L)$, p controls the weight effect of the singular values in defining the norm, which also helps to penalize large singular values less aggressively than the traditional nuclear norm $\sum_i \sigma_i$, leading to better low-rank approximations. This problem is solved using the ADMM approach similar to [27, 35].

2.1. Parameter Estimation

To solve problem 2, we used the Lagrangian multiplier, and we obtained the following result:

$$\mathrm{L}(\mathrm{L,E,Z}) = \gamma \|\mathrm{L}\|_{\mathrm{Log-S}} + \lambda \|\mathrm{E}\|_1 + \langle \mathrm{Z}, \mathrm{M} - \mathrm{L} - \mathrm{E} \rangle + \frac{\mu}{2} \|\mathrm{M} - \mathrm{L} - \mathrm{E}\|_F^2 \tag{4}$$

where Z is the Lagrange multiplier and μ is a penalty parameter. To obtain the optimal updated parameter for the low-rank component L, we first keep the other parameters E and Z constant. We used the ADMM approach [36] to update the parameters sequentially, one at a time.

First, we need to get the optimal updated parameter corresponding to the low rank component L, then we keep all other parameters as a constant, from which the L is updated by:

$$\mathrm{L}^{k+1} = \arg\min_{\mathrm{L}} \gamma \|\mathrm{L}\|_{\mathrm{Log-S}} + \frac{\mu}{2} \left\| \mathrm{M} - \mathrm{L} - \mathrm{E}^k + \mathrm{Z}^k/\mu \right\|_F^2 \tag{5}$$

To solve this problem, let us first denote the term

$$\mathrm{X}^k = \mathrm{M} - \mathrm{E}^k + \frac{\mathrm{Z}^k}{\mu} \tag{6}$$

Then, Equation 4 can be rewritten in the following form:

$$\mathrm{L}^{k+1} = \arg\min_{\mathrm{L}} \gamma \|\mathrm{L}\|_{\mathrm{Log-S}} + \frac{\mu}{2} \|\mathrm{X}^k - \mathrm{L}\|_F^2 \tag{7}$$

Compute the Singular Value Decomposition of X^k:

$$\mathrm{X}^k = U\Sigma V^T \tag{8}$$

where in $X^k = U\Sigma V^T$, X^k represents the original matrix being decomposed. U contains the left singular vectors, with its columns representing directions in the row

space. Σ is a diagonal matrix of singular values, which indicate the magnitude of each component. V^T is the transpose of the right singular vectors, with its columns representing directions in the column space. Apply the log-Schatten thresholding operator similar to the [37,38] from which we can get:

$$\tilde{\Sigma} = \mathrm{T}_{\gamma_1/\mu}(\Sigma) \tag{9}$$

where the log-Schatten shrinkage function is defined as:

$$\mathrm{T}_{\tau}(\sigma_i(\mathrm{L})) = \frac{\sigma_i(\mathrm{L})}{1+\tau/(\sigma_i(\mathrm{L})+\varepsilon)} \tag{10}$$

for each singular value σ_i, where ε is a small positive constant to avoid division by zero. Then, we reconstruct L^{k+1} using the modified singular values:

$$\mathrm{L}^{k+1} = U\tilde{\Sigma}V^T \tag{11}$$

Thus, the final update equation for L is:

$$\mathrm{L}^{k+1} = U\left(\frac{\Sigma}{1+\gamma/(\mu(\Sigma+\varepsilon))}\right)V^T \tag{12}$$

Second to update E, we keep the other variables as constant, then E is updated by

$$\mathrm{E}^{k+1} = \arg\min_{\mathrm{E}} \gamma\|\mathrm{L}\|_1 + \frac{\mu}{2}\left\|\mathrm{M} - \mathrm{L}^{k+1} - \mathrm{E} + \mathrm{Z}^k/\mu\right\|_F^2 \tag{13}$$

Using the soft-thresholding operator:

$$\mathrm{E}^{k+1} = \mathrm{S}_{\lambda/\mu}(\mathrm{M} - \mathrm{L}^{k+1} + \mathrm{Z}^k/\mu) \tag{14}$$

where the soft-thresholding operator [39] is defined as:

$$\mathrm{S}_{\tau}(X) = \mathrm{sign}(X)\, max(\,|X| - \tau, 0) \tag{15}$$

Similarly, the Lagrangian multiplier can be updated using Z and the regularization parameter μ, respectively.

$$\mathrm{Z}^{k+1} = \mathrm{Z}^k + \mu(\mathrm{M} - \mathrm{L}^{k+1} - \mathrm{E}^{k+1}) \tag{16}$$

$$\mu^{k+1} = \rho \cdot \mu^k \tag{17}$$

where ρ is a properly chosen constant and μ is a tunable parameter that adjusts the convergence of the proposed method.

3. DATASET

In this section, we use a publicly available dataset to evaluate the performance of the proposed method through visualization and numerical simulations based on the public availabel datasets. A detailed description of the data is provided in Subsection 1.1.

3.1. Data Description

In our study, we initially used the EyeQ dataset (available at https://github.com/HzFu/EyeQ) to evaluate retinal image data analysis. Next, we expanded our dataset by incorporating a broader set of images from the Kaggle dataset to enhance the diversity and generalizability of our model. We further broadened our analysis by including the STARE dataset (available at https://paperswithcode.com/dataset/stare) and the DRIVE dataset (available at https://paperswithcode.com/dataset/drive), both of which are widely recognized in the field of retinal image analysis and provide high-quality annotated images. We also included the Breast Cancer Image dataset (https://www.kaggle.com/datasets/awsaf49/cbis-ddsm-breast-cancer-image-dataset) to diversify our data and explore the potential of our approach in other medical image domains, enabling us to assess the robustness of our method across different health-related datasets.

We conducted extensive simulations based on the available public databases. First, we considered the Kaggle Database (available at https://www.kaggle.com/datasets/mmazizi/neh-retinal-oct-images), which includes classifications of retinal images based on the severity of diabetes: normal retinal images (without diabetes), mild diabetes, and moderate diabetes. Specifically, there are 305 retinal fundus images representing mild diabetes and 999 retinal fundus images representing moderate diabetes.

The primary purpose of these datasets (retinal and cancer) is to develop and evaluate new methods for the early detection and diagnosis of breast cancer from mammogram images. A detailed summary of the characteristics of the retinal images is provided in Table **2**.

4. SIMULATION RESULTS

In this section, we present the results achieved by the proposed method in comparison to the baseline approaches, RPCA [26] and AWLS-LR [11]. The experimental findings demonstrate the superior performance of our method in terms of noise reduction, feature preservation, and overall image quality, highlighting its effectiveness over existing techniques. The results are presented using two approaches: image quality visualization and numerical evaluation through Peak Signal-to-Noise Ratio (PSNR), Structural Similarity Index Measure (SSIM) and Relative Absolute Error (RAE). In these experimental simulations, we

Table 2: Classification and Count of Retinal Fundus Images

Classification	Description	Count
Without diabetes	Healthy retinal fundus images	1805
Mild diabetes	Mild retinal diabetic cases	305
Moderate diabetes	Moderate retinal diabetic cases	999
Total		**3,109**

used $\gamma = 0.005$ and $\lambda = 1.5$, at which better results were attained. In the following subsection, we first present the ablation results, then conduct image recovery using the proposed method alongside the baseline methods based on the STARE and DRIVE dataset, and finally, we apply the method to cancer data to verify its effectiveness compared to the baseline methods.

4.1. Ablation Studies

4.1.1. STARE Dataset

In this study, we performed an ablation medical image data analysis to evaluate the performance of the proposed method based on the STARE dataset taken from (https://paperswithcode.com/dataset/stare) with each image having a size of 700×605 pixels. First, we applied RPCA with Log-Schatten Norm alone, followed by RPCA with both Log-Schatten Norm and AHE, as illustrated in Figure **1**. The results demonstrate that the combination of both techniques significantly enhances the details in retinal fundus images, leading to better noise reduction and improved feature preservation compared to using Log-Schatten Norm alone. The image quality for visualization is more consistent based on the statistical measures mainly PSNR and SSIM, as shown in Table **3**.

4.1.2. DRIVE Dataset

Similarly, we also tried to further conduct the ablation study based on the DRIVE (available at https://paperswithcode.com/dataset/drive) retinal images with each 584×565 pixels, from which the recovered images by the combination of the Log-Schatten Norm and AHE is more detailed the retinal fundus images as compared with the Log-Schatten Norm alone. This result is given in Figure **2**. This results are more consistent based on the statistical measures mainly PSNR and SSIM, as shown in Table **3**.

4.1.3. Mild and Moderate Retinal Image Data Analysis

Similarly, we also tried to carry out the ablation study based on the mild retinal fundus images with each 224×224 pixels, from which the images recovered by the combination of LSN and AHE are more detailed the retinal fundus images compared to LSN alone. This result is given in Figure **3**. The AHE is more essential in describing the detail characteristics of retinal iamges compared to LSN alone.

Similarly, we also tried to further conduct the ablation study based on moderate retinal fundus images with each 224×224 pixels, from which the images recovered by the combination of LSN and AHE are more detailed than the retinal fundus images compared to LSN alone. This result is shown in Figure **4**, where the enhanced image is clearer in detailing the blood vessels as compared to the RPCA with LSN alone

4.2. Comparison of Methods

4.2.1. STARE and DRIVE Retinal Image Data Analysis

After conducting the ablation studies, we compared the proposed method with the baseline methods RPCA [26] and AWLS-LR [11] based on the STARE dataset. The results show that the proposed method outperforms the baseline methods in recovering retinal fundus images as given in Figure **5**. This finding is consistent with the results presented in Table **4**. This indicates that the proposed method is more resilient to artifacts and better at recovering high-dimensional retinal images.

Similarly, we compared the proposed method with the baseline methods RPCA [26] and AWLS-LR [11] based on the DRIVE dataset. The results show that the proposed method outperforms the baseline methods in recovering retinal fundus images, as shown in Figure **6**. The images recovered by the proposed method demonstrate better enhancement of the degraded images compared to the baseline methods [11,26]. This is due to the incorporation of the LSN along with AHE, which makes the new method more resilient to artifacts. This finding is consistent with the results presented in Table **4**.

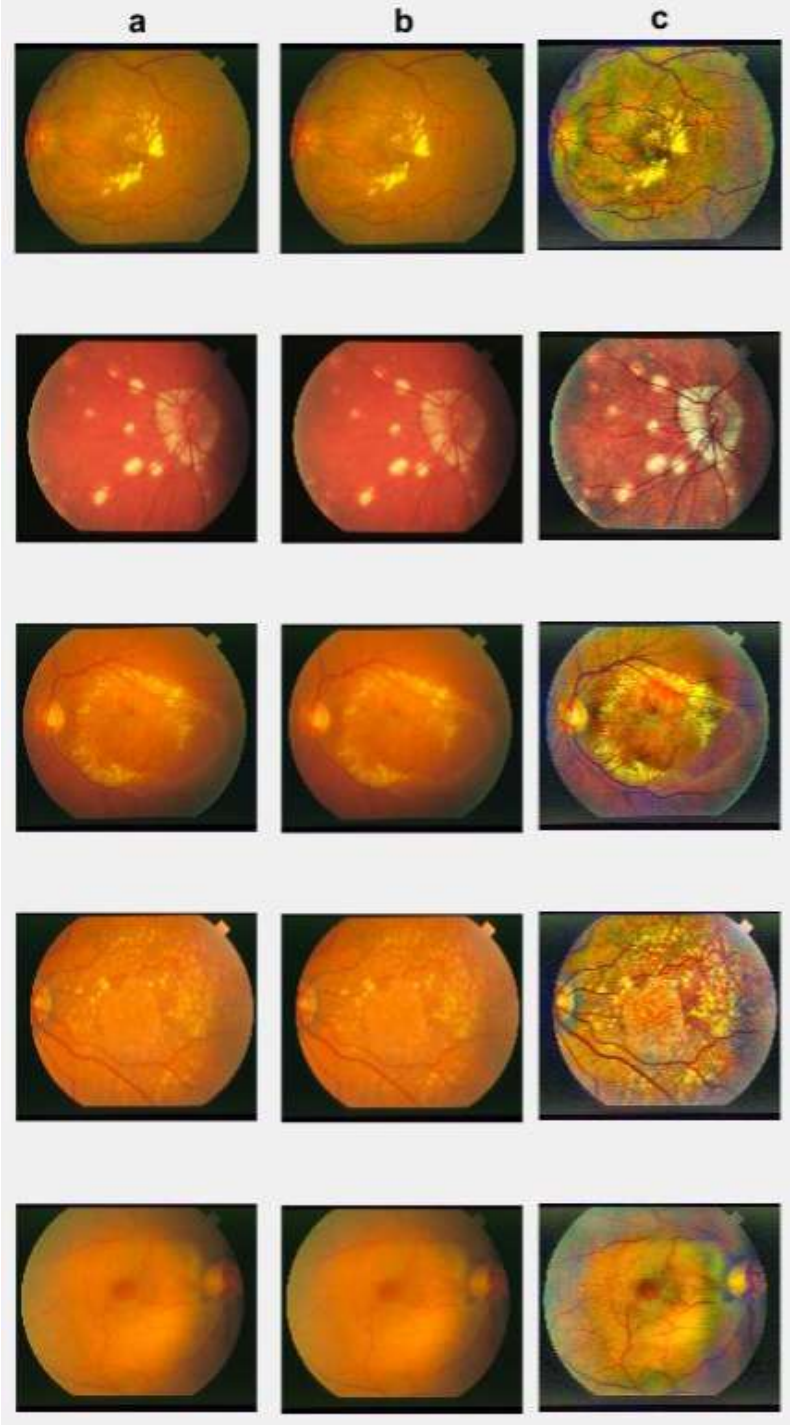

Figure 1: Retinal Image Enhancement based on the STARE dataset (**a**) Degraded; (**b**) RPCA Log-Schatten Norm; (**c**) RPCA Log-Schatten Norm and AHE.

Table 3: Comparison of PSNR, SSIM, and RAE for STARE and DRIVE Datasets

Methods	STARE Data			DRIVE Data		
	PSNR	SSIM	RAE	PSNR	SSIM	RAE
Proposed method	15.89	0.60	0.46	17.18	0.5357	0.3890
RPCA [26]	17.26	0.69	0.43	18.52	0.5571	0.3651
AWLS-LR [11]	23.32	0.86	0.16	19.33	0.7779	0.2623

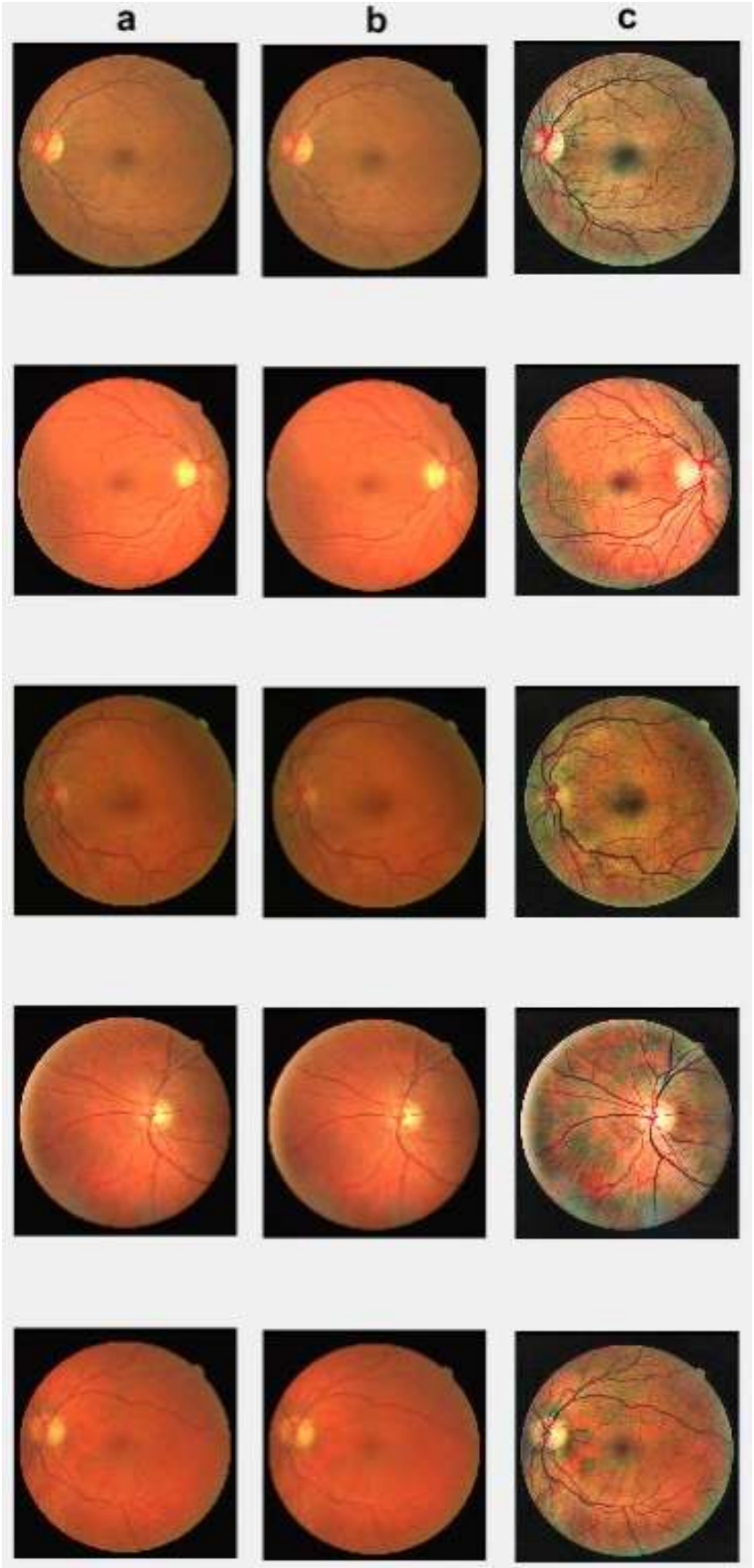

Figure 2: Retinal Image Enhancement based on the DRIVE dataset (**a**) Degraded; (**b**) RPCA Log-Schatten Norm; (**c**) RPCA Log-Schatten Norm and AHE.

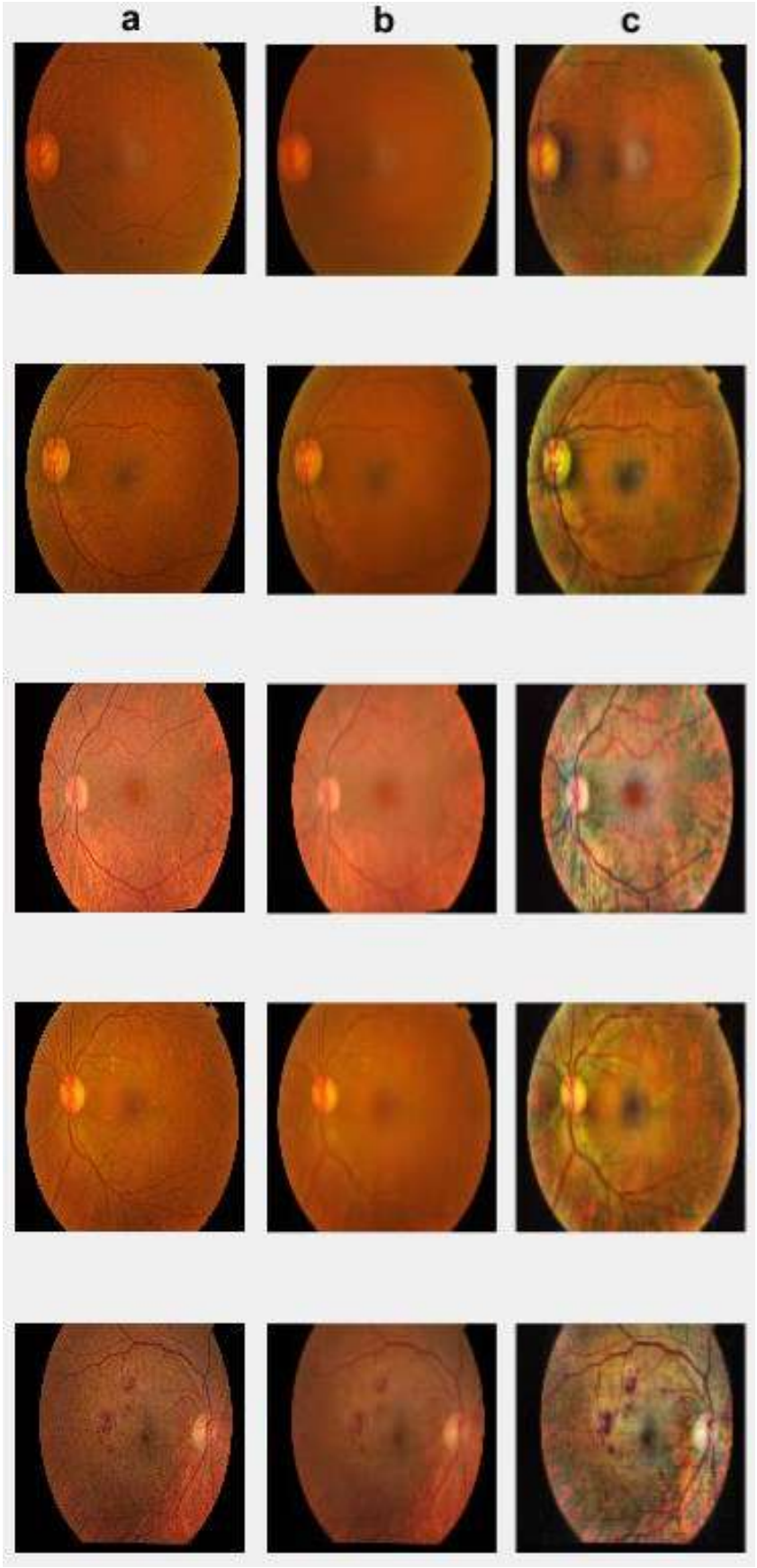

Figure 3: Mild Retinal Image Enhancement based on the Kaggle dataset (**a**) Degraded; (**b**) RPCA Log-Schatten Norm; (**c**) RPCA Log-Schatten Norm and AHE.

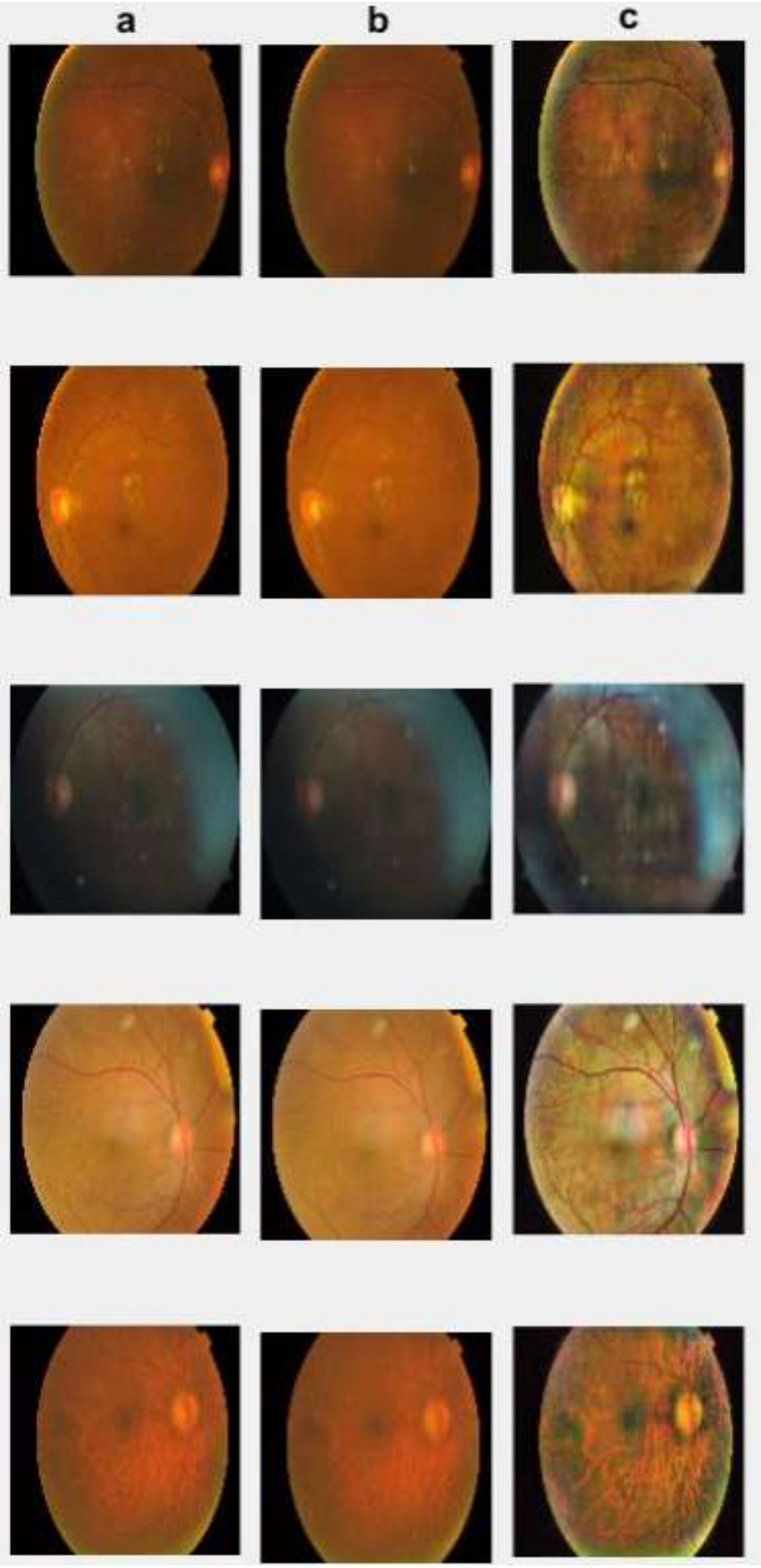

Figure 4: Moderate Retinal Image Enhancement based on the Kaggle dataset (**a**) Degraded; (**b**) RPCA Log-Schatten Norm; (**c**) RPCA Log-Schatten Norm and AHE.

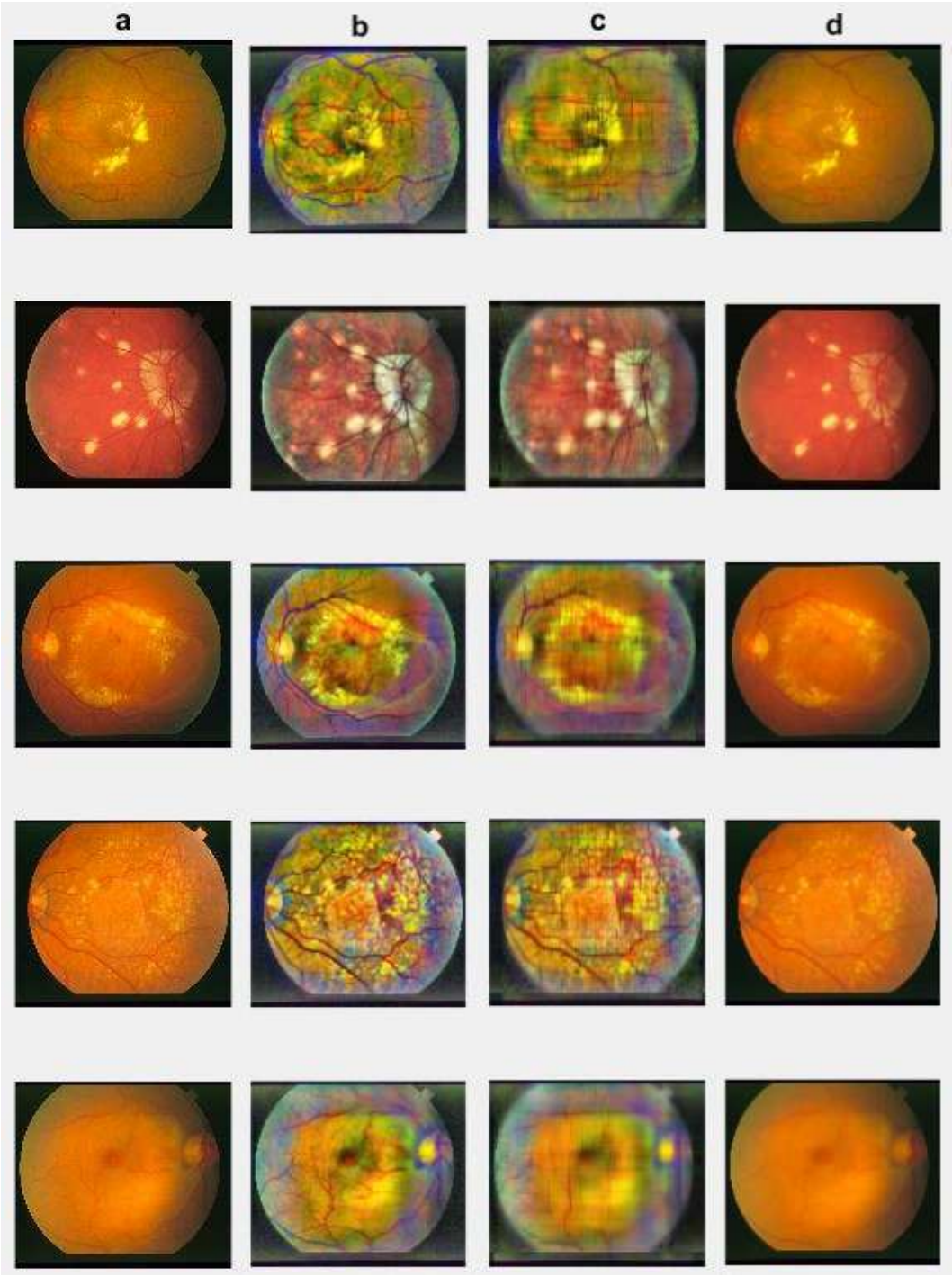

Figure 5: Retinal Image Enhancement based on the STARE dataset (**a**) Degraded; (**b**) Proposed Method; (**c**) RPCA [26] and AWLS-LR [11].

Table 4: PSNR, SSIM and RAE for Cancer Data

2*Methods	Malignant			Benign		
	PSNR	SSIM	RAE	PSNR	SSIM	RAE
Proposed method	12.67	0.5829	0.4151	13.90	0.5995	0.3275
RPCA [26]	13.49	0.6183	0.4045	14.48	0.6192	0.3173
AWLS-LR [11]	19.21	0.5272	0.1923	18.86	0.4692	0.1631

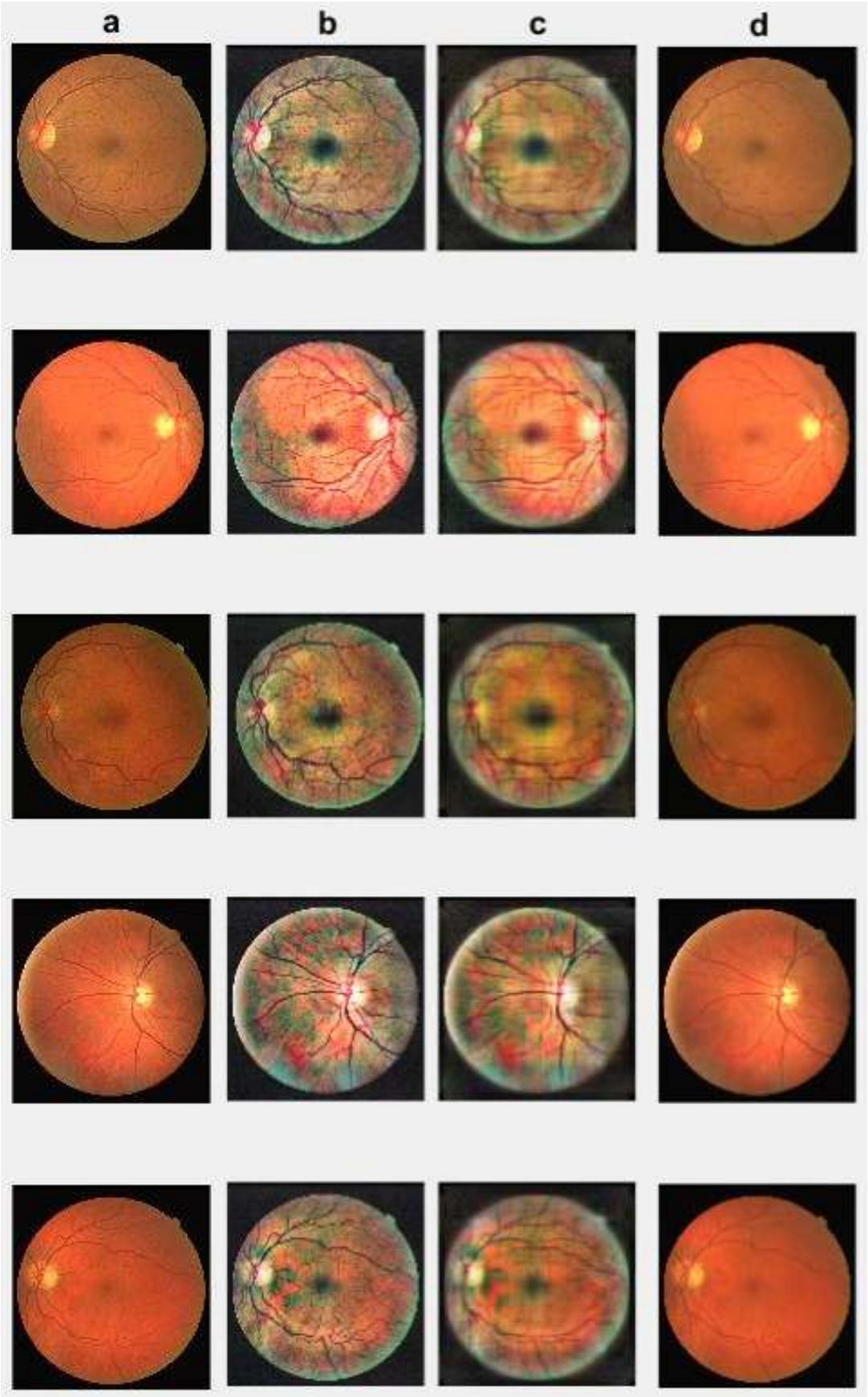

Figure 6: Retinal Image Enhancement based on the DRIVE dataset (**a**) Degraded; (**b**) Proposed Method; (**c**) RPCA [26] and AWLS-LR [11].

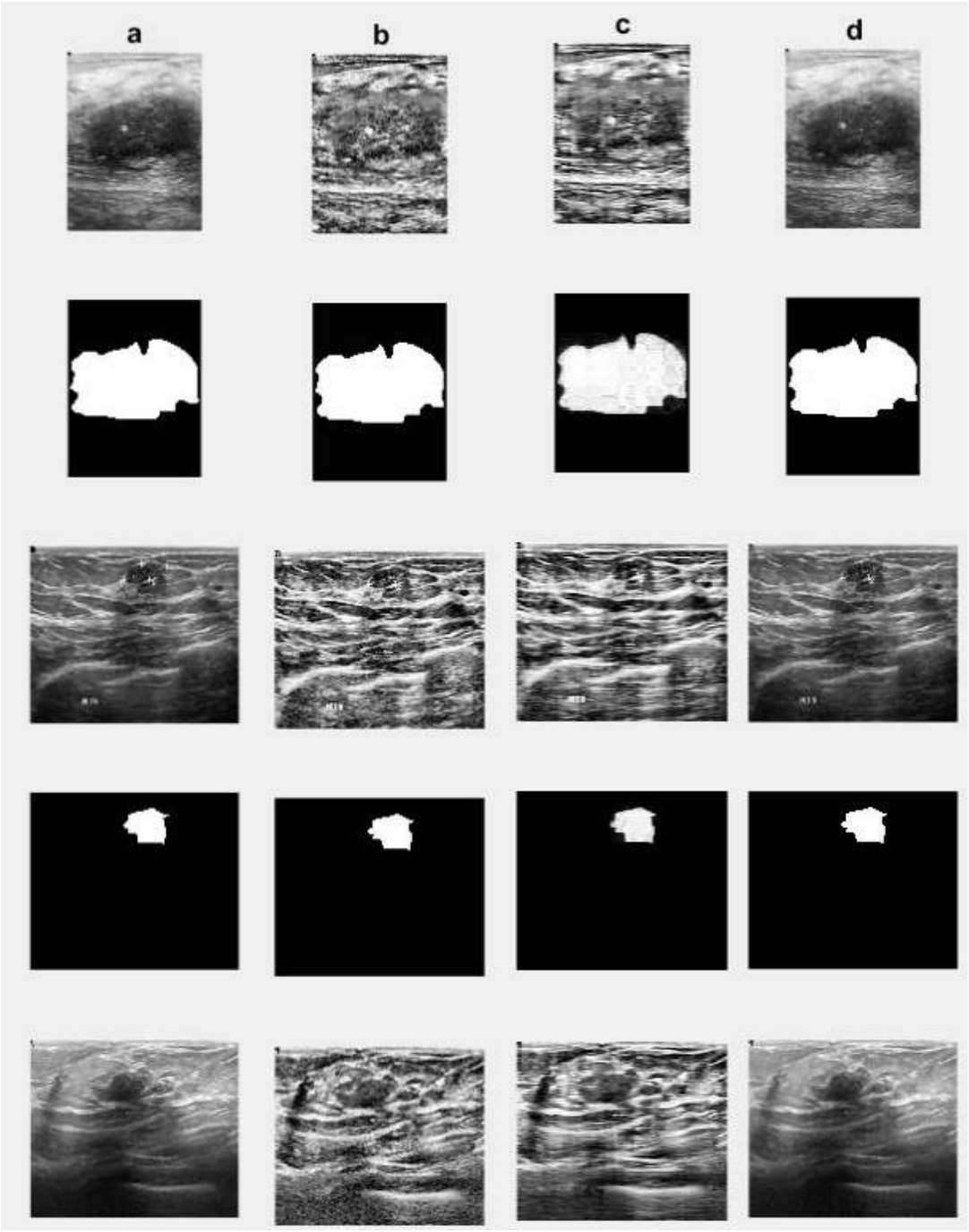

Figure 7: Malignant Cancer Image enhancement based on the Kaggle dataset (**a**) Degraded; (**b**) Proposed Method; (**c**) RPCA [26] and AWLS-LR [11].

4.2.2. Malignant Cancer Image Data Analysis

The proposed RPCA with LSN demonstrates superior performance in enhancing malignant cancer images compared to existing methods such as RPCA [26] and AWLS-LR [11]. While the degraded image suffers from severe noise, low contrast, and structural distortions that obscure critical diagnostic features, the proposed method effectively suppresses noise while preserving fine tumor details. Unlike RPCA [26], which over-smooths the image and removes essential tumor features, or AWLS-LR [11], which leaves residual noise, the LSN adaptively retains significant singular values, ensuring better contrast, sharper tumor boundaries, and improved morphological structure visibility. This leads to more precise differentiation between malignant tissues and surrounding regions, ultimately enhancing diagnostic accuracy in medical imaging. This result is given in Figure **7** and this result is more consistent with the numerical simulations given in Table **4**.

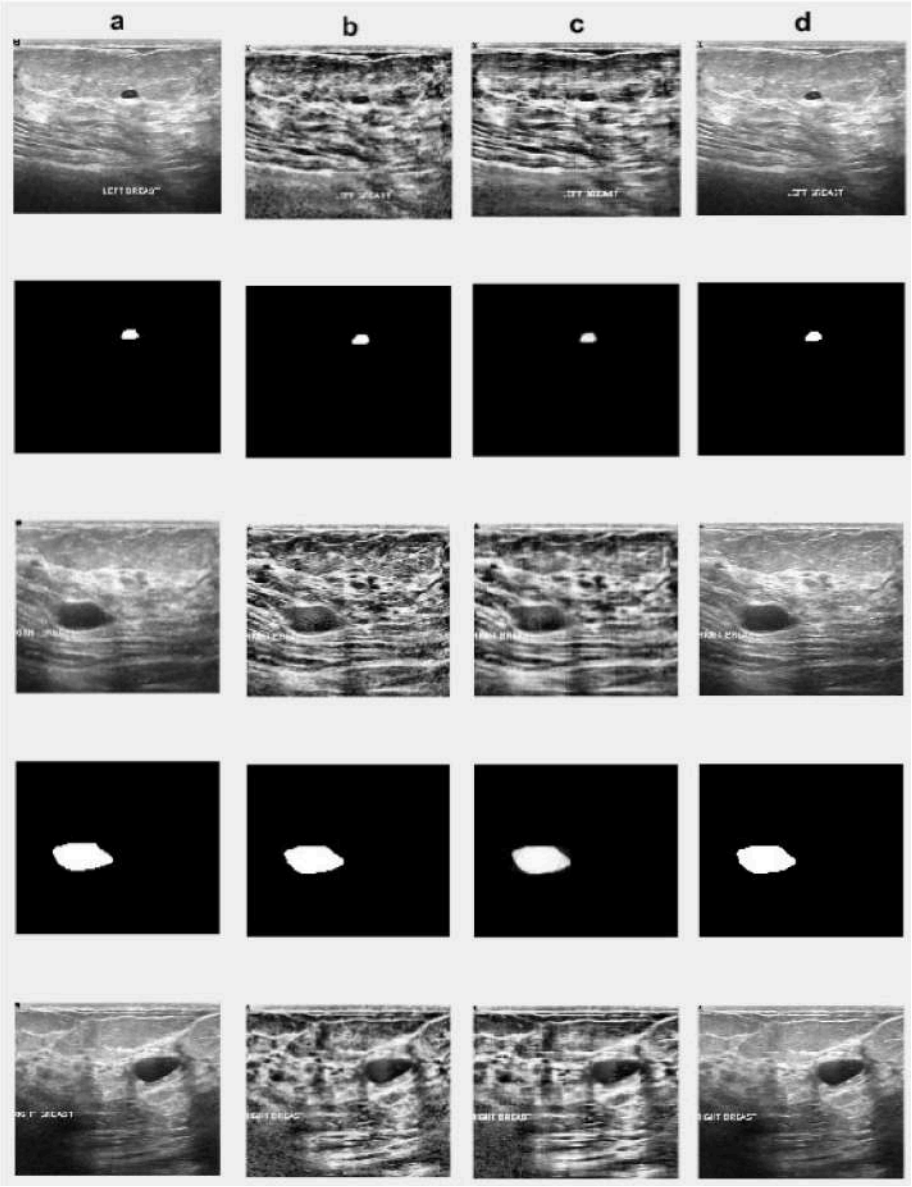

Figure 8: Benign Cancer Image Enhancement based on the Kaggle dataset (**a**) Degraded; (**b**) Proposed Method; (**c**) RPCA [26] and AWLS-LR [11].

4.2.3. Benign Cancer Image Data Analysis

The proposed RPCA with Log-Schatten Norm significantly enhances benign cancer images, outperforming existing methods such as RPCA [26] and AWLS-LR [11]. In the degraded image (a), severe noise, low contrast, and structural distortions obscure critical diagnostic features, making accurate identification of benign tumors challenging. The proposed method (b) RPCA with Log-Schatten Norm effectively suppresses noise while preserving fine tumor structures and enhancing local contrast, resulting in clearer visualization of benign regions. In contrast, (c) RPCA [26] tends to over-smooth the image, leading to loss of important diagnostic details, while AWLS-LR [11] struggles to fully eliminate residual noise, leaving unwanted artifacts that can affect clinical interpretation. By adaptively retaining significant singular values, the Log-Schatten Norm ensures sharper tumor boundaries, improved morphological structure visibility, and enhanced contrast, facilitating more precise differentiation between benign tumors and surrounding healthy tissue. The effectiveness of the proposed approach is visually demonstrated in Figure **7**, while numerical simulations in Table **4** further validate its robustness and superior performance.

5. CONCLUSION AND FUTURE WORK

The pioneering RPCA method [34] was originally developed for image recovery, providing a powerful tool

for separating low-rank and sparse components in images. Since its introduction, various scholars [21,26, 40,41] have continuously enhanced the method to improve its performance. For example, several modifications have been proposed [26] to address challenges such as noise, outliers, and computational efficiency, resulting in more robust and accurate techniques for medical image recovery. These advancements have significantly broadened the applicability of RPCA in fields such as medical imaging, video surveillance, and remote sensing, where high-quality image recovery is essential.

Despite its potential, however, there is a lack of literature connecting RPCA to medical image research, presenting an opportunity for further exploration and integration of RPCA techniques in medical imaging, particularly for early diagnosis and disease detection. In this paper, we propose a novel RPCA framework that incorporates the LSN and AHE for medical image data analysis. The LSN effectively addresses the limitations of traditional low-rank regularization techniques, such as the nuclear norm and log-weighted nuclear norm, by adaptively preserving significant singular values while reducing noise and artifacts. This leads to superior low-rank approximation and enhanced robustness in image recovery. Additionally, AHE improves local contrast, further enhancing image quality for diagnostic applications.

The entire problem is formulated as an optimization task, and the optimization process is efficiently handled using ADMM, ensuring computational stability and convergence. Experimental results demonstrate that the proposed method outperforms state-of-the-art techniques in medical image analysis, making it a promising tool for improving disease detection, including diabetic retinopathy and cancer diagnosis.

6. ETHICAL CONSIDERATIONS

This study utilizes publicly available datasets from reputable sources, including the DRIVE, STARE, Kaggle, and EyeQ databases. These datasets provide a valuable foundation for the development and evaluation of our methods. We confirm that all data used in this research are publicly accessible and do not involve any personally identifiable information, ensuring compliance with ethical standards. The use of these datasets adheres to the terms and conditions set by their respective providers, and no additional ethical approval is required for their utilization in this study.

REFERENCES

[1] Ahmad I, Singh VP, Gore MM. Detection of diabetic retinopathy using discrete wavelet-based center-symmetric local binary pattern and statistical features. Journal of Imaging Informatics in Medicine 2024; 1-28. https://doi.org/10.1007/s10278-024-01243-2

[2] Besag J, York J, Mollie A. Bayesian image restoration, with two applications in spatial statistics. Annals of the institute of Statistical Mathematics 1991; 43: 1-20. https://doi.org/10.1007/BF00116466

[3] Künsch HR. Robust priors for smoothing and image restoration. Annals of the Institute of Statistical Mathematics 1994; 46: 1-19. https://doi.org/10.1007/BF00773588

[4] Zhu H, Li T, Zhao B. Statistical learning methods for neuroimaging data analysis with applications. Annual review of Biomedical Data Science 2023; 6(1): 73-104. https://doi.org/10.1146/annurev-biodatasci-020722-100353

[5] Gianfrancesco MA, Goldstein ND. A narrative review on the validity of electronic health record-based research in epidemiology. BMC Medical Research Methodology 2021; 21(1): 234. https://doi.org/10.1186/s12874-021-01416-5

[6] Farag AA. Biomedical image analysis: Statistical and variational methods. Cambridge University Press 2014. https://doi.org/10.1017/CBO9781139022675

[7] Feng L, Wang J. Projected robust pca with application to smooth image recovery. Journal of Machine Learning Research 2022; 23(249): 1- 41.

[8] Nie F, Wu D, Wang R, Li X. Truncated robust principle component analysis with a general optimization framework. IEEE Transactions on Pattern Analysis and Machine Intelligence 2020; 44(2): 1081-1097. https://doi.org/10.1109/TPAMI.2020.3027968

[9] Raunig DL, McShane LM, Pennello G, Gatsonis C, Carson PL, Voyvodic JT, *et al*. Quantitative imaging biomarkers: a review of statistical methods for technical performance assessment. Statistical Methods in Medical Research 2015; 24(1): 27-67. https://doi.org/10.1177/0962280214537344

[10] Webb-Vargas Y, Chen S, Fisher A, Mejia A, Xu Y, Crainiceanu C, Caffo B, Lindquist MA. Big data and neuroimaging. Statistics in Biosciences 2017; 9: 543-558. https://doi.org/10.1007/s12561-017-9195-y

[11] Li K, Wen Y-W, Xiao X, Zhao M. Robust pca based on adaptive weighted least squares and low-rank matrix factorization 2024; arXiv preprint arXiv: 2412.14629. https://doi.org/10.2139/ssrn.5191156

[12] Naz H, Ahuja NJ. A novel contrast enhancement technique for diabetic retinal image pre-processing and classification. International Ophthalmology 2024; 45(1): 11. https://doi.org/10.1007/s10792-024-03377-2

[13] Zhou H, Li L, Zhu H. Tensor regression with applications in neuroimaging data analysis. Journal of the American Statistical Association 2013; 108(502): 540-552. https://doi.org/10.1080/01621459.2013.776499

[14] Fu Y, Wang C, Wang Y, Chen B, Peng Q, Wang L. Automatic detection of longitudinal changes for retinal fundus images based on low-rank decomposition. Journal of Medical Imaging and Health Informatics 2018; 8(2): 284-294. https://doi.org/10.1166/jmihi.2018.2110

[15] Ong F, Lustig M. Beyond low rank+ sparse: Multiscale low rank matrix decomposition. IEEE Journal of Selected Topics in Signal Processing 2016; 10(4): 672-687. https://doi.org/10.1109/JSTSP.2016.2545518

[16] Otazo R, Candes E, Sodickson DK. Low-rank plus sparse matrix decomposition for accelerated dynamic mri with separation of background and dynamic components. Magnetic resonance in medicine, 73(3): 1125-1136, 2015. https://doi.org/10.1002/mrm.25240

[17] Changfa Shi, Yuanzhi Cheng, Jinke Wang, Yadong Wang, Kensaku Mori, and Shinichi Tamura. Low-rank and sparse decomposition based shape model and probabilistic atlas for

automatic pathological organ segmentation. Medical Image Analysis 2017; 38: 30-49. https://doi.org/10.1016/j.media.2017.02.008

[18] Wang J, Lu C-H, Liu J-X, Dai L-Y, Kong X-Z. Multi-cancer samples clustering via graph regularized low-rank representation method under sparse and symmetric constraints. BMC Bioinformatics 2019; 20: 1-15. https://doi.org/10.1186/s12859-019-3231-5

[19] Liu F, Huang W. Esdiff: a joint model for low-quality retinal image enhancement and vessel segmentation using a diffusion model. Biomedical Optics Express 2023; 14(12): 6563-6578. https://doi.org/10.1364/BOE.506205

[20] Wang L, Schaefer A. Diagnosing diabetic retinopathy from images of the eye fundus. cs230 2020; 14.

[21] Likassa HT, Chen D-G, Kewei Chen, Yalin Wang, and Wenhui Zhu. Robust pca with lw, and l2, 1 norms: A novel method for low-quality retinal image enhancement. Journal of Imaging 2024; 10(7): 151. https://doi.org/10.3390/jimaging10070151

[22] Chandrasekaran V, Sanghavi S, Parrilo PA, Willsky AS. Sparse and low-rank matrix decompositions. IFAC Proceedings Volumes 2009; 42(10): 1493-1498. https://doi.org/10.3182/20090706-3-FR-2004.00249

[23] Wang J, Li Y-J, Yang K-F. Retinal fundus image enhancement with image decomposition and visual adaptation. Computers in Biology and Medicine 2021; 128: 104116. https://doi.org/10.1016/j.compbiomed.2020.104116

[24] Zhou M, Jin K, Wang S, Ye J, Qian D. Color retinal image enhancement based on luminosity and contrast adjustment. IEEE Transactions on Biomedical Engineering 2017; 65(3): 521-527. https://doi.org/10.1109/TBME.2017.2700627

[25] Sükei E, Rumetshofer E, Schmidinger N, Mayr A, Schmidt-Erfurth U, Klambauer G, Bogunović H. Multimodal representation learning in retinal imaging using self-supervised learning for enhanced clinical predictions. Scientific Reports 2024; 14(1): 26802. https://doi.org/10.1038/s41598-024-78515-y

[26] Likassa HT, Chen DG, Sun D. A novel rpca method using log-weighted nuclear and l2, 1 norms combined with contrastlimited adaptive histogram equalization (clahe) for high dimensional natural and medical image data. International Journal of Statistics in Medical Research 2024; 13: 275-290. https://doi.org/10.6000/1929-6029.2024.13.25

[27] Likassa HT, Chen D-G. Robust principal component analysis for retinal image enhancement. In Biostatistics Modeling and Public Health Applications Springer 2024; 12: 157-190. https://doi.org/10.1007/978-3-031-69690-9_7

[28] Bie C, Liang Y, Zhang L, Zhao Y, Chen Y, Zhang X, He X, Song X. Motion correction 11 of chemical exchange saturation transfer mri series using robust principal component analysis (rpca) and pca. Quantitative Imaging in Medicine and Surgery 2019; 9(10): 1697. https://doi.org/10.21037/qims.2019.09.14

[29] Mohammed S, Masotti M, Osher N, Acharyya S, Baladandayuthapani V. Statistical analysis of quantitative cancer imaging data. Statistics and Data Science in Imaging 2024; 1(1): 2405348. https://doi.org/10.1080/29979676.2024.2405348

[30] Santos CS, Amorim-Lopes M. Externally validated and clinically useful machine learning algorithms to support patient-related decision-making in oncology: a scoping review. BMC Medical Research Methodology 2025; 25(1): 45. https://doi.org/10.1186/s12874-025-02463-y

[31] Tibrewala R, Dutt T, Tong A, Ginocchio L, Lattanzi R, Keerthivasan MB, *et al*. Fastmri prostate: A public, biparametric mri dataset to advance machine learning for prostate cancer imaging. Scientific Data 2024; 11(1): 404. https://doi.org/10.1038/s41597-024-03252-w

[32] Kamarudin AN, Cox T, Kolamunnage-Dona R. Time-dependent roc curve analysis in medical research: current methods and applications. BMC Medical Research Methodology 2017; 17: 1-19. https://doi.org/10.1186/s12874-017-0332-6

[33] Lin Z, Chen M, Ma Y. The augmented lagrange multiplier method for exact recovery of corrupted low-rank matrices 2010; arXiv preprint arXiv: 1009.5055.

[34] Candès EJ, Li X, Ma Y, Wright J. Robust principal component analysis? Journal of the ACM 2011; 58(3): 1-37. https://doi.org/10.1145/1970392.1970395

[35] Likassa HT, Fang W-H, Leu J-S. Robust image recovery via affine transformation and l {2, 1} norm. IEEE Access 2019; 7: 125011-125021. https://doi.org/10.1109/ACCESS.2019.2932470

[36] Boyd S, Parikh N, Chu E, Peleato B, Eckstein J. Distributed optimization and statistical learning via the alternating direction method of multipliers. Foundations and Trends® in Machine Learning 2011; 3(1): 1-122. https://doi.org/10.1561/2200000016

[37] Nie F, Huang H, Ding C. Low-rank matrix recovery via efficient schatten p-norm minimization. In Proceedings of the AAAI Conference on Artificial Intelligence 2012; 26: 655-661. https://doi.org/10.1609/aaai.v26i1.8210

[38] Xie Y, Gu S, Liu Y, Zuo W, Zhang W, Zhang L. Weighted schatten p-norm minimization for image denoising and background subtraction. IEEE Transactions on Image Processing 2016; 25(10): 4842-4857. https://doi.org/10.1109/TIP.2016.2599290

[39] Loris I, Verhoeven C. On a generalization of the iterative soft-thresholding algorithm for the case of non-separable penalty. Inverse Problems 2011; 27(12): 125007. https://doi.org/10.1088/0266-5611/27/12/125007

[40] Likassa HT. New robust principal component analysis for joint image alignment and recovery via affine transformations, frobenius and l2, 1 norms. International Journal of Mathematics and Mathematical Sciences 2020; 2020(1): 8136384. https://doi.org/10.1155/2020/8136384

[41] Likassa HT, Fang W-H, Chuang Y-A. Modified robust image alignment by sparse and low rank decomposition for highly linearly correlated data. In 3rd International Conference on Intelligent Green Building and Smart Grid 2018; pp. 1-4. https://doi.org/10.1109/IGBSG.2018.8393549

Received on 13-03-2025 Accepted on 09-04-2025 Published on 03-05-2025

https://doi.org/10.6000/1929-6029.2025.14.27